International Journal of Solids and Structures 50 (2013) 4333–4340

Contents lists available at ScienceDirect

International Journal of Solids and Structures

journal homepage: www.elsevier.com/locate/ijsolstr

Effect of adhesive thickness, adhesive type and scarf angle on the mechanical properties of scarf adhesive joints

Lijuan Liao [a,*], Chenguang Huang [a], Toshiyuki Sawa [b]

[a] Key Laboratory for Mechanics in Fluid Solid Coupling Systems, Institute of Mechanics, Chinese Academy of Sciences, Beijing 100190, People's Republic of China
[b] Graduate School of Engineering, Hiroshima University, 1-4, Kagamiyama, Higashihiroshima, Hiroshima 739-8527, Japan

ARTICLE INFO

Article history:
Received 19 June 2013
Received in revised form 16 July 2013
Available online 11 September 2013

Keywords:
Adhesive thickness
Adhesive Type
Scarf adhesive joint (SJ)
Cohesive zone model (CZM)
Scarf angle

ABSTRACT

The effects of adhesive thickness, adhesive type and scarf angle, which are determined as the main control parameters by the dimensional analysis, on the mechanical properties of a scarf adhesive joint (SJ) subjected to uniaxial tensile loading are examined using a mixed-mode cohesive zone model (CZM) with a bilinear shape to govern the interface separation. Particularly, the adhesive-dependence of the vital cohesive parameters of CZM, which mainly include initial stiffness, total fracture energy and separation strength, is introduced emphatically. The numerical results demonstrate that the ultimate tensile loading increases as the adhesive thickness decreases. Cross the ultimate tension, the joint loses the load-bearing capacity when adopting the brittle adhesive but sustains partial load-bearing capacity while selecting the ductile adhesive. In addition, for the joint with the ductile adhesive, the maximum applied displacement until the complete failure of it is directly proportional to the adhesive thickness, which is different from the case using the brittle adhesive. Taking the combination of the ultimate loading and applied displacement into account, failure energy is employed to evaluate the joint performances. The results show that the failure energy of the joint with the brittle adhesive increases as the adhesive thickness decreases. Conversely, the situation of the joint using the ductile adhesive is vice versa. Moreover, the effect of the adhesive thickness becomes more noticeable with decreasing the scarf angle owing to the variation of the proportion of each component of the mixed-mode. Furthermore, all the characteristic parameters (the ultimate tensile loading, the maximum applied displacement and the failure energy) that adopted to describe the performances of SJ increase as the scarf angle decreases. Finally, the numerical method employed in this study is validated by comparing with existing experimental results.

1. Introduction

With the ability to transfer loadings more efficiently and provide higher strength than the lap-shear counterpart, the scarf adhesive joint (SJ) is widely used in modern structural technology (Gacoin et al., 2009; Hamit, 2012; Kimiaeifar et al., 2012; Sou-Hsiung and Reaz, 2011). Correspondingly, examinations of mechanical properties are crucial to technological applications of SJ subjected to external loadings, especially in the aerospace and automotive industries.

Among all the influential factors, the adhesive thickness has an important effect on the mechanical properties of the adhesive joint (Afendi et al., 2011; Chai, 2004; Kahraman et al., 2008; Lucas et al., 2006, 2009; Banea and Lucas, 2009; Marzi et al., 2011; Xu and Wei, 2013a). Experience shows that the lap joint strength increases as the adhesive layer gets thinner (Lucas et al., 2006, 2009). However, as opinions vary, no unanimous conclusion can be drawn. The broad observations obtained by the previous investigations are not applicable to all cases as there are other variables involved (Lucas et al., 2006, 2008), such as the type of loading, the diversity of geometrical configurations, the type of constraint and the type of adhesive (ductile or brittle) (Banea and Lucas, 2009). In the writing of Adams et al., 1997, the strength of the single lap adhesive joint (SLJ) is given by the load corresponding to the total plastic deformation if the adhesive is ductile. However, for more brittle adhesives, this conclusion is not suitable for the work carried out by Adams et al. In addition, as a prominent geometric characteristic of SJ, the scarf angle including its effect on the strength of the joint under uniaxial tensile loading has been investigated by many studies (Afendi et al., 2011; Hamit, 2012; He et al., 2009, 2010), the results of which showed that the failure loadings increase as the angle decreases.

Abbreviations: SJ, scarf adhesive joint; CZM, cohesive zone model; SLJ, single lap adhesive joint; T–S, traction–separation.

* Corresponding author. Address: Key Laboratory for Mechanics in Fluid Solid Coupling Systems, Institute of Mechanics, Chinese Academy of Sciences, No.15, Beisihuan West Road, Beijing 100190, People's Republic of China. Tel.: +86 10 8254 4291; fax: +86 10 8254 4256.

E-mail addresses: liaohuanxin@hotmail.com, liao_angelica@yahoo.com (L. Liao).

0020-7683/$ - see front matter © 2013 Elsevier Ltd. All rights reserved.
http://dx.doi.org/10.1016/j.ijsolstr.2013.09.005

Nomenclature

E_n: Young's modulus ($n = adh$, adherend; $n = ad$, adhesive) (GPa)
G_n: shear modulus ($n = ad$, adhesive) (GPa)
v_n: Poisson's ratio ($n = adh$, adherend; $n = ad$, adhesive)
σ_y: adhesive yield strength (MPa)
σ_f: adhesive fracture strength (MPa)
A_c: area under the stress-strain curve of the adhesive (MPa)
G_{i0}: instinct cohesive energy for mode i (i = I, II) (N/mm)
k_i: initial stiffness in CZM (i = I, II) (MPa/mm)
G_{ic}: total fracture energy in CZM (i = I, II) (N/mm)
$\sigma_{u,i}$: separation strength in CZM (i = I, II) (MPa)
G_{ip}: plastic dissipation energy of adhesive layer for mode i (i = I, II) (N/mm)
$r_{ip}^{max}(90°)$: maximum value of plastic zone height for mode i (i = I, II) (mm)
t_n: thickness ($n = adh$, adherend; $n = ad$, adhesive) (mm)
l: length of the long edge of the adherend (mm)
w: adherend (joint) width (mm)
θ: joint scarf angle
F_y: resultant force of the uniaxial tensile loading along the y-direction per unit thickness of the joint (kN)
s_y: applied displacement along the y-direction (mm)
F_u: ultimate value of the uniaxial tensile loading along the y-direction per unit thickness of the joint (kN)
s_m: maximum value of the applied displacement along the y-direction (mm)

As mentioned above, it can be observed that a number of parameters, such as adhesive thickness, adhesive type and scarf angle, influence the mechanical properties of SJ collectively but not individually.

The overall performance of SJ could be obtained with taking into account the failure behavior of the adhesive layer, which has been demonstrated that it takes place progressively as energy dissipates gradually at the crack tip (Adams et al., 1997; Afendi et al., 2011; Campilho et al., 2009; Liechti and Freda, 1989; Lucas et al., 2006; Mohammed and Liechti, 2000; Xu and Wei, 2012, 2013a,b). Considering the elastic-plastic deformation behavior together with the cohesive damage and failure of the adhesive layer, cohesive zone model (CZM) is an ideal alternative analysis method to perform the failure evaluation comparing with the conventional elastic-plastic models (de Moura et al., 2008; Ridha et al., 2011). In addition, with the advantages of mesh independence and dispensable initial crack, CZM is a powerful approach to capture the behaviors of the structure up to failure (Mohammed and Liechti, 2000; Gustafson and Waas, 2009; Pardoen et al., 2005; Rudawska, 2010) based on a traction–separation (T–S) law, which can be considered as a representation of the constitutive relation of the adhesive layer (Marzi et al., 2011; Xu and Wei, 2013a).

In the present study, the effects of adhesive thickness, adhesive type and scarf angle, which are determined as the main control parameters through the dimensional analysis, on the mechanical properties of SJ subjected to uniaxial tensile loading are examined using a mixed-mode CZM with a bilinear shape coupled with finite element subroutine (performed in ABAQUS®). Particularly, the influences of adhesive thickness on the cohesive parameters, which mainly include initial stiffness, total fracture energy and separation strength, are discussed emphatically. Furthermore, the performance of SJ under uniaxial tensile loading, which are principally described utilizing ultimate applied tensile loading, applied displacement until the complete failure and stretch energy of the tensile loading, are analyzed through evaluating the influences imposed by the three main control parameters mentioned above.

2. Dimensional analysis

A physical model of SJ, in which the same metallic adherends are bonded together utilizing the adhesive with the scarf angle θ, is shown in Fig. 1. In order to capture the main control parameters that influence the performances of SJ under uniaxial tensile loading, dimensional analysis is carried out.

Owing to the very great difference in stiffness between the adherend and the adhesive (Gacoin et al., 2009) in SJ, progressive nonlinear failure occurs at the adhesive interface (Liechti and Freda, 1989). Subsequently, the evolution of the progressive failure can be simulated by adopting CZM, which is considered as the constitutive law of the adhesive layer (Marzi et al., 2011; Xu and Wei, 2013a). Governed by T–S law (bilinear for simplicity as shown in Fig. 2) in each pure mode (i = I, II), total fracture energy G_{ic} and separation strength $\sigma_{u,i}$ play the key roles in demonstrating the interface separation behavior with insignificant effect of the precise shape (Freund and Suresh, 2003). Furthermore, owing to not perpendicular to the applied tensile loading of the oblique adhesive interface, a complex stress state of the joint is present with mixed-mode (mode I and II) damage propagation, which is also shown in Fig. 2 (Campilho et al., 2009; Lucas et al., 2006).

Subjected to uniaxial tensile loading, the ultimate tensile loading F_u is affected by three categories of system parameters: the material parameters of adhesive (total fracture energy G_{Ic} and G_{IIc}, and separation strength $\sigma_{u,I}$ and $\sigma_{u,II}$), the material parameters of metallic adherend (Young's modulus E_{adh} and Poisson's ratio v_{adh}) and the geometrical parameters of SJ (adhesive thickness t_{ad}, scarf angle θ , long edge length of adherend l and width w). Correspondingly, F_u is expressed by the function of the three categories of system parameters mentioned above as following,

$$F_u = f(\underbrace{G_{Ic}, G_{IIc}, \sigma_{u,I}, \sigma_{u,II}}_{properties\ of\ adhesive};\ \underbrace{E_{adh}, v_{adh}}_{properties\ of\ adherend};\ \underbrace{t_{ad}, \theta, l, w}_{geomentry}) \quad (1)$$

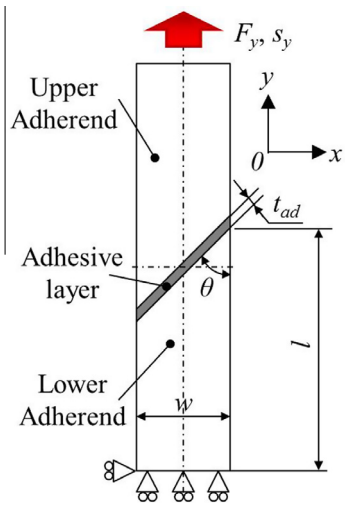

Fig. 1. A model of SJ under uniaxial tensile loading with dimensions and boundary conditions.

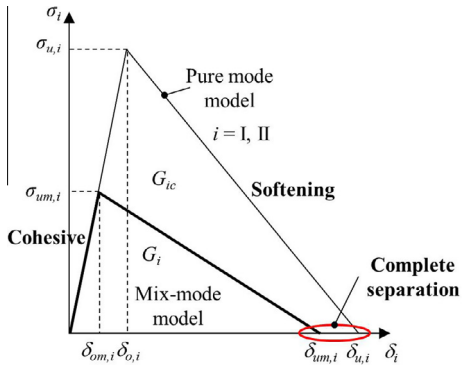

Fig. 2. Pure and mixed-mode damage model (Lucas et al., 2006).

The non-dimensional-normalized form is

$$\frac{F_u}{\sigma_{u,I} t_{ad}} = f\left(\underbrace{\frac{G_{Ic}}{\sigma_{u,I} t_{ad}}, \frac{G_{IIc}}{G_{Ic}}, \frac{\sigma_{u,II}}{\sigma_{u,I}}}_{\text{properties of adhesive}}; \underbrace{\frac{E_{adh}}{\sigma_{u,I}}, \nu_{adh}}_{\text{properties of adherend}} ; \underbrace{\theta, \frac{l}{t_{ad}}, \frac{w}{t_{ad}}}_{\text{geomentry}} \right) \tag{2}$$

For the first category system factors, $G_{Ic}/(\sigma_{u,I} t_{ad})$ indicates the ratio between the separation displacement and the thickness of the adhesive layer. In addition, G_{IIc}/G_{Ic} and $\sigma_{u,II}/\sigma_{u,I}$ represent the extent of the anisotropy of the adopted adhesive between mode I and II, which are the intrinsic characteristics of the given adhesive. Therefrom, the adhesive type is an influential factor. Furthermore, all the cohesive parameters are proved with the characteristic of adhesive thickness-dependence (Lee et al., 2004; Pardoen et al., 2005; Xu and Wei, 2013a). Thus, the adhesive thickness t_{ad} is also determined as one of the control factors.

As for the second category ones, they are determined only by the chosen adhesive when the material of the adherend is fixed. Consequently, the effects of adherend are not taken into account in the analysis for a given material.

As regards the factors of the last category, comparing with the long edge length l and the width w of the adherend, the adhesive thickness t_{ad} is a quite small magnitude ($l/t_{ad} \gg 1$, $w/t_{ad} \gg 1$). The two normalized variables are decided by the length l and width w, which are fixed in the present study. Without doubt, the scarf angle θ should be determined as a control parameter, which decides the stress state at the adhesive interface and influences the proportion of each mode of mixed-mode as well.

Accordingly, the adhesive thickness t_{ad}, the adhesive type and the scarf angle θ are determined as the main control parameters, whose effects on the performances of SJ are examined in the present study.

3. Numerical analysis

3.1. Details of the simulation model

Geometrical and material nonlinear numerical analysis is performed in ABAQUS® to simulate the mechanical properties of SJ with various adhesive thicknesses, adhesive types and scarf angles subjected to uniaxial tensile loading. The equivalent simulation model is shown in Fig. 1. The adherend is 27.7 mm in width (w) and 92.0 mm in the length of the long edge (l) (He et al., 2009, 2010). In addition, to examine the effect on the performances of the joint, the scarf angle is chosen as $\theta = 30°, 45°$ and $60°$, respectively. The actual thickness of the adhesive layer denoted as t_{ad}, which is different from the geometrical thickness during modeling, is introduced to the cohesive parameters described in Section 3.3.

Generally, the width of the joint is considerably larger than the thickness (the thin plate specimen). Consequently, SJ under uniaxial tensile loading is simplified as a 2D plane-strain problem in the present study. Cartesian coordinates (x, y) are adopted in modeling. As shown in Fig. 1, the boundary conditions are: 1) the free end of the lower adherend is constrained both in x- and y-direction; 2) the tensile loading F_y, which is simulated by controlling displacement increment method along the y-direction (s_y), is applied to the free end of the upper adherend.

The adherends, which adopt the material parameters of high-strength steel (He et al., 2010; He et al., 2009), are defined as the isotropic elastic model using Young's modulus E_{adh} = 209 GPa and Passion's ratio ν_{adh} = 0.29, respectively. In addition, the models of the adherends are meshed using four-node quadrilateral plane strain elements. Meanwhile, in order to analyze the effect of the type of adhesive, two different adhesives are selected: a comparatively brittle adhesive (AV138/HV998) and a comparatively ductile adhesive (Hysol EA 9361) (Lucas et al., 2006). The adhesive layer is built as a single layer using four-node cohesive elements, which share nodes with the neighboring elements of the adherends. Dense mesh using biasing effects is provided in the adhesive region while a sparse spare mesh is employed in other regions for higher computational accuracy. CZM is adopted to simulate damage initiation and growth. The parameters of the cohesive elements will be discussed in Section 3.3. Furthermore, optional viscous damping is implemented between node pairs to improve convergence (Gustafson and Waas, 2009).

3.2. Details of CZM

To define the progressive nonlinear cohesive interactions along fracture surfaces, a bilinear (Chandra et al., 2002; Ghosh et al., 2000; Li and Chandra, 2003) CZM is adopted based on T–S laws (Campilho et al., 2009; Gustafson and Waas, 2009; Lucas et al., 2006; Park and Paulino, 2011; Rudawska, 2010; Xu and Wei, 2012, 2013a,b) to characterize the interface separation behavior (Sørensen and Kirkegaard, 2006).

Implemented into the ABAQUS® commercial code as a user subroutine, the formulation is based on a constitutive relationship between stresses and relative displacements (Campilho et al., 2009; Lucas et al., 2006; Xu and Wei, 2013a). Then, it can be noticed that the stresses of the interface finite element before damage onset are calculated using:

$$\boldsymbol{\sigma} = \mathbf{D}\boldsymbol{\delta} \tag{3}$$

where $\boldsymbol{\sigma}$, $\boldsymbol{\delta}$ and $\mathbf{D}$ are the vector of interface finite element stresses, the vector of relative displacements and a diagonal matrix containing the interface stiffness, respectively. For each pure mode, the material softens progressively with damage when the displacement δ_i is over $\delta_{o,i}$. The softening relationship is described as:

$$\boldsymbol{\sigma} = (\mathbf{I} - \mathbf{E})\mathbf{D}\boldsymbol{\delta} \tag{4}$$

where $\mathbf{I}$ is the identity matrix, and $\mathbf{E}$ is a diagonal matrix containing the damage parameters defined by:

$$e_i = \frac{\delta_{u,i}(\delta_i - \delta_{o,i})}{\delta_i(\delta_{u,i} - \delta_{o,i})} \tag{5}$$

where δ_i is the current relative displacement in mode i and $\delta_{o,i}$ is the displacement corresponding to the onset of damage. The maximum relative displacement $\delta_{u,i}$ of complete separation is obtained by equating the area under the soften curve with the respective critical fracture energy:

$$G_{ic} = 1/2\sigma_{u,i}\delta_{u,i} \tag{6}$$

Under mixed-mode conditions, damage initiation is controlled by using a quadratic stress criterion as following,

$$(\sigma_I/\sigma_{u,I})^2 + (\sigma_{II}/\sigma_{u,II})^2 = 1 \tag{7}$$

which assumes that a pure compressive deformation or stress state does not initiate damage.

It is assumed that a linear fracture criterion determines the damage propagation, which could be expressed as:

$$G_I/G_{Ic} + G_{II}/G_{IIc} = 1 \tag{8}$$

The fracture energy in each mode of complete failure is described using the area of the triangle in Fig. 2:

$$G_i = 1/2\sigma_{um,i}\delta_{um,i} \tag{9}$$

The relative displacements for each mode corresponding to damage onset $\delta_{om,i}$ and ultimate failure $\delta_{um,i}$ can be expressed as:

$$\delta_{om,i} = \frac{\beta_i\delta_{om}}{\sqrt{1+\beta_{II}^2}} \tag{10}$$

$$\delta_{um,i} = \frac{\beta_i\delta_{um}}{\sqrt{1+\beta_{II}^2}} \tag{11}$$

where β_i is the mode ratios ($\beta_i = \delta_i/\delta_I$); δ_{om}, δ_{um} are the equivalent mixed-mode relative displacements, which are shown as following:

$$\delta_{om} = \delta_{o,I}\delta_{o,II}\sqrt{\frac{1+\beta_{II}^2}{\delta_{o,II}^2 + \beta_{II}^2\delta_{o,I}^2}} \tag{12}$$

$$\delta_{um} = \frac{1+\beta_{II}^2}{\delta_{om}\left(\frac{1}{\delta_{o,I}\delta_{u,I}} + \frac{\beta_{II}^2}{\delta_{o,II}\delta_{u,II}}\right)} \tag{13}$$

The damage parameters can be obtained by substituting Eqs. (12) and (13) to Eq. (5).

3.3. Adhesive thickness-dependence of cohesive parameters

A parameterized bilinear T–S law for mixed-mode is used to model de-cohesion of SJ by defining three cohesive parameters to capture the progressive failure of the adhesive. In each pure mode, three cohesive parameters to define the control triangle of the bilinear T–S curve are: initial stiffness (the slope of the linear ascent of T–S curve), total fracture energy (the enveloped area of T–S curve) and separation strength (the peak stress value of T–S curve) (Lee et al., 2010). Influenced by the adhesive thickness, all the cohesive parameters, whose the subscripts denoting each pure mode are omitted for simplicity, are represented as the functions of the adhesive thickness t_{ad} (Xu and Wei, 2013a).

In CZM, the thickness of the adhesive layer t_{ad} is introduced to the stiffness matrix **D** (Lucas et al., 2006), in which each matrix element is the initial stiffness in each pure mode (mode I and II). The initial stiffness, which is an analogy with the stiffness coefficient of spring, is employed to define the ratio between the cohesive stress and separation displacement before the adhesive damage occurs (Gustafson and Waas, 2009). In each pure mode (mode I and II), the initial stiffness is expressed as following, respectively (Gustafson and Waas, 2009; Xu and Wei, 2013a).

$$\begin{aligned} k_{\mathrm{I}} &= \frac{E_{ad}}{t_{ad}} \\ k_{\mathrm{II}} &= \frac{G_{ad}}{t_{ad}} \end{aligned} \tag{14}$$

where E_{ad} and G_{ad} mean the Young's modulus and the shear modulus of the adhesive, respectively. It can be seen that the initial stiffness in each pure mode (mode I and II) varies inversely with the adhesive thickness t_{ad} for each type of adhesive.

Xu and Wei (2013a) pointed out that the adhesive layer, which was considered as an equivalent cohesive layer, would dissipate two types of energies (intrinsic cohesive energy G_0 and plastic dissipation energy G_p) (Swadener and Liechti, 1998; Swadener et al., 1999; Mello and Liechti, 2006) with a certain thickness. They provided the total fracture energy expression as shown in Eq. (15):

$$G_c = G_0 + G_{\mathrm{p}} = \begin{cases} G_0 + A_c t_{ad} & (t_{ad} < 2r_{\mathrm{p}}^{\max}(90^\circ)) \\ G_0 + 2A_c r_{\mathrm{p}}^{\max}(90^\circ) & (t_{ad} \geqslant 2r_{\mathrm{p}}^{\max}(90^\circ)) \end{cases} \tag{15}$$

where G_0 is considered as intrinsic work of fracture associated with the embedded cohesive zone. Meanwhile, G_p is denoted as the contribution to the bond toughness arising from the plastic dissipation and stored elastic energy within the adhesive layer (Pardoen et al., 2005). In addition, as shown in Eq. (15), the expression of the total fracture energy is piecewise function satisfying various conditions related to the thickness t_{ad}. Essentially, the plastic dissipation G_p is significantly influenced by the maximum value of plastic zone height $r_p^{max}(90^\circ)$ when the crack plane is assumed in the middle of the adhesive layer (Lee et al., 2004; Pardoen et al., 2005; Xu and Wei, 2013a). When $t_{ad} < 2r_p^{max}(90^\circ)$, the plastic dissipation energy G_p is approximately estimated as $t_{ad}A_c$ (Wei and Zhao, 2008; Xu and Wei, 2013b; Xu and Wei, 2012), where A_c is the area below the stress-strain curve of the bulk adhesive. Thus, the plastic dissipation energy is considered as the mean plastic work per unit adhesive volume. Once $t_{ad} \geqslant 2r_p^{max}(90^\circ)$, the plastic dissipation energy G_p would maintain as a constant value, which is dominated by $2A_c r_p^{max}(90^\circ)$.

Furthermore, the separation strength σ_u, which is expressed as a function of adhesive thickness t_{ad}, is also obtained by Xu and Wei (2013a) as:

$$\frac{\sigma_u}{\sigma_f} = \begin{cases} \sqrt{\frac{1+\eta\left(\frac{t_{ad}}{t_c}\right)}{(1+\eta)\left(\frac{t_{ad}}{t_c}\right)}} & (t_{ad} < t_c) \\ 1 & (t_{ad} \geqslant t_c) \end{cases} \tag{16}$$

where t_c is defined as the critical thickness of the adhesive layer with the expression of $t_c = 2r_p^{max}(90^\circ)$. In addition, η ($\eta = t_{ad}A_c/G_0$) is introduced as a dimensionless parameter. Moreover, σ_f is the bulk fracture strength of the adhesive. The potential physical meaning of Eq. (16) is that the separation strength σ_u would be identical to the bulk fracture strength σ_f when the adhesive thickness t_{ad} reaches the critical value t_c (Ji et al., 2010, 2011, 2012).

In order to examine the effect of adhesive thickness on the performance of SJ under uniaxial tensile loading, a series of thickness t_{ad} should be set in advance. According to previous investigations (Ji et al., 2010, 2011, 2012; Lucas et al., 2006; Xu and Wei, 2013a), the upper limit of the adhesive thickness t_{ad} is selected as 1.0 mm. Thus, three thicknesses (0.1 mm, 0.5 mm and 1.0 mm) are discussed in the present study.

Based on the adhesive thickness-dependence mentioned above, the necessary cohesive parameters can be determined by the constitutive parameters of adopted adhesives as shown in Table 1. Consequently, the cohesive parameters are obtained for a series of adhesive thicknesses, which are shown in Table 2. Particularly,

Table 1
Adhesive constitutive parameters (Lucas et al., 2006).

Parameters	AV138/HV998 (brittle)	Hysol EA 9361 (ductile)
E_{ad} (GPa)	4.59	0.67
v_{ad}	0.35	0.4
σ_y (MPa)	36.49	4.23
σ_f (MPa)	41.01	7.99
A_c (MPa)	0.36	2.69
G_{I0} (N/mm)	0.3	2.61
G_{II0} (N/mm)	0.6	5.22

Table 2
Adhesive thickness-dependence cohesive parameters.

Variables	Adhesive type					
	AV138/HV998 (brittle)			Hysol EA 9361 (ductile)		
t_{ad} (mm)	0.1	0.5	1.0	0.1	0.5	1.0
k_I (MPa/mm)	45900	9180	4590	6700	1340	670
k_{II} (MPa/mm)	17000	3400	1700	2393	478.6	239.3
$\sigma_{u,I}$ (MPa)	76.73	41.01	41.01	25.89	13.57	11.11
$\sigma_{u,II}$ (MPa)	105.57	52.28	41.01	35.74	17.48	13.57
G_{Ic} (N/mm)	0.34	0.48	0.48	2.88	3.96	5.30
G_{IIc} (N/mm)	0.64	0.78	0.96	5.49	6.57	7.91

with the critical thickness t_c = 0.5 mm of AV138/HV998 in mode I, the separation strength $\sigma_{u,I}$ and the total fracture energy G_{Ic} keep as constants out of the critical thickness range. By obtaining computing method of cohesive parameters, which are affected by the adhesive thickness, the simulations of SJ under uniaxial tensile loading can be carried out using FEM.

4. Results and discussions

4.1. Numerical results

At the first stage of the loading procedure, the uniaxial tensile loading F_y increases up to the peak value, which is defined as the ultimate loading denoted as F_u. Thereafter, it drops to zero as the applied displacement s_y increases constantly owing to the damage of the adhesive layer. Correspondingly, the maximum displacement at the point of the complete failure is defined and labeled as s_m.

Fig. 3 shows the variation of the applied tensile loading F_y with the displacement s_y of SJs adopting various adhesive thickness t_{ad}, adhesive types and scarf angles θ, in which F_y is the resultant force of the uniaxial tensile loading along the y-direction per unit thickness of the joint. Similar to the system of springs in series, the upper and lower adherends connected with the adhesive layer. Conrespondingly, it is assumed that the stiffness of the adhesive joint can be represented using the slope of the ascent stage of the load-displacement curve. The evolutionary processes of the applied loadings F_y of the joints choosing the brittle and ductile adhesives are similar, both including ascent and descent stages. However, the downward trends are different from each other. For the joint with the brittle adhesive, after reaching the peak, the applied loading F_y drops to zero sharply with less plastic deformation. On the other hand, in the case of the joint adopting the ductile adhesive, the tensile loading F_y decreases quite slowly experiencing long displacement until to final failure.

Fig. 4 shows the variation of the ultimate loading F_u with the scarf angle θ for different adhesive thicknesses and adhesive types. With the increment of the adhesive thickness t_{ad}, the ultimate loading F_u decreases in all cases discussed in this study. In addition, in the case of the joint adopting the brittle adhesive, the variation of the maximum displacement s_m until the complete failure of the joint with respect to the adhesive thickness t_{ad} is ill defined as shown in Fig. 3(a). Conversely, for the joint with the ductile adhesive, the maximum displacement s_m until the complete failure of the joint is directly proportional to the adhesive thickness t_{ad} regularly as shown in Fig. 3(b). Furthermore, all the loading components decrease as the scarf angle θ increases.

4.2. Consequential discussions

In the simulated model, CZM is selected to describe the separation behavior of the adhesive joint controlled by initial stiffness, total fracture energy and separation strength (Xu and Wei, 2013a; Xu and Wei, 2013b; Xu and Wei, 2012). As the peak value of T–S curve, the separation strength σ_u limits the maximum threshold. Correspondingly, governed by the separation strength of the chosen adhesive, the ultimate loading F_u of SJ is larger when using the brittle adhesive (AV138/HV998) than that selecting the ductile adhesives (Hysol EA 9361), which can be observed from Figs. 3 and 4. To examine the monotonicity of the separation strength σ_u function varying with the adhesive thickness t_{ad} as shown in Eq. (14), it is necessary to differentiate it as following:

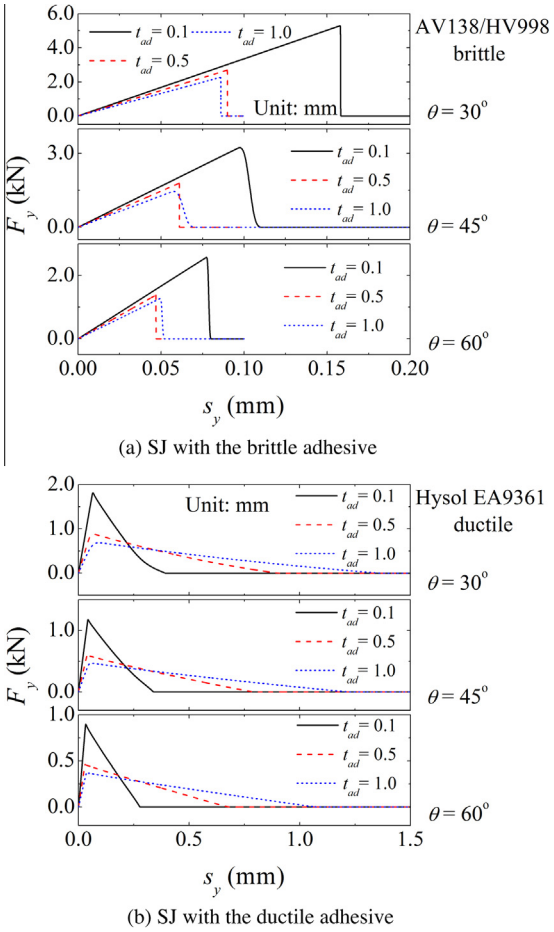

Fig. 3. Loading-displacement curves of SJ.

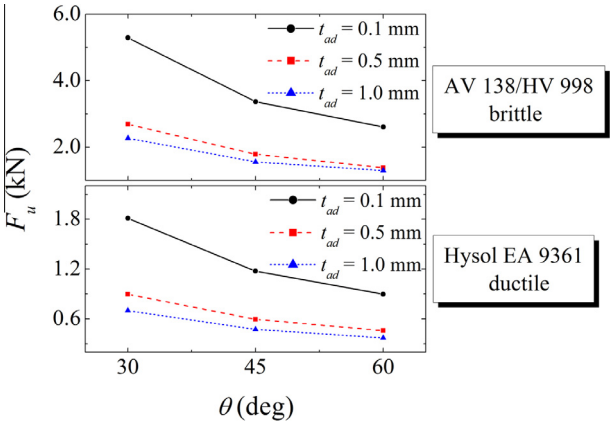

Fig. 4. Variation of the ultimate loading F_u with the scarf angle θ for different adhesive thicknesses and adhesive types.

$$\frac{\partial \sigma_u}{\partial t_{ad}} = \begin{cases} \frac{\sigma_f G_0 (A_c t_{ad}^2 - 2A_c t_c t_{ad} - G_0 t_c)}{t_{ad}^2 (A_c t_{ad} + G_0)^2} \sqrt{\frac{A_c t_{ad}^2 + G_0 t_c}{t_{ad}(A_c t_{ad} + G_0)}} & (t_{ad} < t_c) \\ 0 & (t_{ad} \geqslant t_c) \end{cases} \tag{17}$$

It can be obtained that the first partial derivative of the separation strength σ_u with respect to the adhesive thickness t_{ad} is held as negative in the range $t_{ad} < t_c$. Correspondingly, it is concluded that the separation strength σ_u monotonically decreases with increases in the adhesive thickness t_{ad}. Subsequently, it is easy to understand that the ultimate loading F_u of the joint increases as the adhesive thickness t_{ad} decreases in each case of given scarf angle.

Owing to the effect of adhesive type, as shown in Fig. 3, the downward trends of the tensile loadings show the differences between the cases of the joints with the brittle and ductile adhesive. As the result from the damage of the adhesive layer, the decline is controlled by the total fracture energy of the selected adhesive. In the study of Lucas et al. (2006), the tensile stress-strain curves of the brittle adhesive AV138/HV998 and the ductile adhesive Hysol EA 9361 were provided. It can be obtained that the brittle adhesive AV138/HV998, which is sensitive to defects without any noticeable voids at the failure surface, has no plastic deformation when reaching the ultimate strength. Conversely, for the ductile adhesive Hysol EA 9361 with high ductility, the stress-sensitivity is so low that can be ignored after the maximum stress is achieved. On another aspect, as listed in Table 2, with the increasing of the adhesive thickness t_{ad}, the total fracture energy of each pure mode increases for both two types of adhesive. However, the definite values of the brittle adhesive AV138/HV998 are one order of magnitude less than the corresponding ones of the ductile adhesive Hysol EA 9361.

As for the load-bearing capacity of SJ, the ultimate loading F_u is usually proposed to estimate it (Lucas et al., 2006; Xu and Wei, 2012). However, the ultimate loading F_u corresponds neither to the crack initiation nor to the onset of instability (Yang and Thouless, 2001; Xu and Wei, 2013a). Furthermore, as shown in Fig. 3, the variation of the applied displacement with the adhesive thickness t_{ad} for the joint adopting the brittle adhesive shows different properties from that for the joint choosing the ductile adhesive. For the joint using brittle adhesive as shown in Fig. 3(a), without plastic deformation, it totally loses the load-bearing capacity in the decline process of the tensile loading F_y. Contrary, partial load-bearing capacity of the joint employing the ductile adhesive is sustained even during the drop procedure unless the tensile loading F_y reaches zero, which can be seen in Fig. 3(b).

Only employing the ultimate loading F_u to evaluate the performances of the adhesive joint is not sufficient. Actually, the ultimate loading $F_u$combined with the maximum applied displacement s_m govern the mechanical properties of SJ. In the present study, the necessary energy resulting in the joint failure, which is described utilizing the work done by the applied loading according to the displacement until the complete failure occurs is introduced to evaluate the joint performances as shown in Eq. (18).

$$E_f = \int_0^{s_m} F_y ds_y \tag{18}$$

Fig. 5 shows the variation of the failure energy E_f with the scarf angle θ for different adhesive thicknesses and adhesive types. Under a given scarf angle, the failure energy E_f of the joint selecting the ductile adhesive improves accompanying with the thickening of adhesive thickness t_{ad}, which is opposite to the situation of the joint choosing the brittle adhesive. In addition, it can also be seen that the difference of the failure energy E_f resulted from the effect of the adhesive thickness t_{ad} under the condition of the given scarf angle becomes more noticeable as the scarf angle θ decreases. With the enhancement of the level of mix-mode as the scarf angle θ decreases, the effect of adhesive thickness t_{ad} on the mechanical properties of the SJ is more significant. Naturally, the discussions of the effect of the adhesive thickness t_{ad} are not exceeding the range of critical thickness t_c for each type of adhesive.

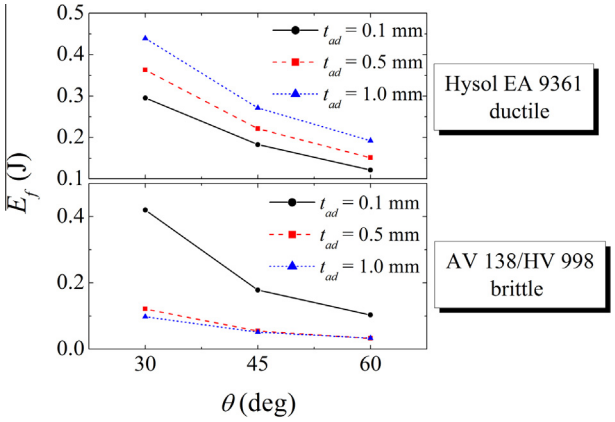

Fig. 5. Variation of the failure energy E_f with the scarf angle θ for different adhesives thicknesses and adhesive types.

5. Conclusions

In the present study, through dimensional analysis, adhesive thickness, adhesive type and scarf angle are determined as the main control parameters that influence the performances of SJ. Correspondingly, the examinations of the effects of these main control factors on the mechanical properties of SJ subjected to uniaxial tensile loading are performed using a mixed-mode CZM with a bilinear shape coupled with finite element subroutine. The adhesive-dependence of the vital cohesive parameters of CZM (initial stiffness, total fracture energy and separation strength) is introduced emphatically based on the existing results. The numerical results demonstrate that the ultimate tensile loading F_u increases as the adhesive thickness t_{ad} decreases. Cross the ultimate tension, the joint loses the load-bearing capacity when adopting the brittle adhesive while it sustains partial load-bearing capacity when selecting the ductile adhesive owing to the effects of the adhesive type. In addition, for the joint with the ductile adhesive, the maximum applied displacement until the complete failure is directly proportional to the adhesive thickness, which is different from the case of the joint adopting the brittle adhesive. To evaluate the joint performances more comprehensively and effectively, the failure energy is employed, which is defined by the work done by the tensile loading with respect to the applied displacement until the complete failure. The results show that the failure energy of the joint with the brittle adhesive increases as the adhesive thickness t_{ad} decreases. Conversely, the variation trend of the failure energy of the joint using the ductile adhesive is vice versa. Moreover, the effect of the adhesive thickness t_{ad} becomes more noticeable as the scarf angle θ decreases owing to the change of the proportion of each pure mode of the mixed-mode. Furthermore, the parameters describing the performances of SJ, which mainly include the ultimate tensile loading, the maximum applied displacement and the failure energy, increase as the scarf angle θ decreases.

Acknowledgments

This work is supported by the National Natural Science Foundation of China, Grant No. 11202222. The theoretical support from Prof. Wei Yueguang, Dr. Xu Wei and Dr. Wang Yiwei (Institute of Mechanics, Chinese Academy of Sciences) are also appreciated.

Prof. Xi Wang is gratefully acknowledged for providing language help.

Appendix A. Validation of the present simulated method

The numerical results are compared with the results from the existing experimental measurements to validate the present method. The normalized ultimate tensile loading $F_u/t_{adh}w\sigma_y$ varing with the scarf angle θ can be seen in Fig. A1.

In the study carried out by Afendi et al. (2011), a commercial brittle epoxy adhesive with the trademark of Hi-Super30 was used to join dissimilar adherends with scarf angle $\theta = 45°, 60°$ and 75°, respectively. The target bond thickness of the adhesive layer in their study was designed in the range from 0.1 mm to 1.0 mm. The loading-displacement results of the adhesive thickness $t_{ad} = 0.1$ mm and 1.0 mm are chosen to compare with the present results. Correspondingly, the adherend thickness t_{adh}, the width of the joint w and the yield stress of the given adhesive $\sigma_y$were designed as 5 mm, 40 mm and 34.76 MPa in their work, respectively.

In addition, the study performed by Gacoin et al. (2009) is additionally referred. The adhesive used in their work was an epoxy resin SIKADUR 30 COLLE® (SIKA, Paris, France). The desired adhesive thickness t_{ad} was 0.5 mm. The results of the SJ under tensile loading with the scarf angle $\theta = 33°$ and 18° are selected as the comparative objects. Correspondingly, the adherend thickness t_{adh}, the width of the joint w and the yield stress of the given adhesive $\sigma_y$were chosen as 10 mm, 10 mm and 24 MPa, respectively.

According to the existing results in the previous investigations (Afendi et al., 2011; Gacoin et al., 2009), to cover all situations mentioned in references in the present study, the scarf angle θ is set as 15°, 30°,45°, 60°, 75° and 90°, respectively. Furthermore, the numerical results of the joint with the brittle adhesive thickness $t_{ad} = 0.1$ mm, 0.5 mm and 1.0 mm are compared with the existing experimental measurements as mentioned above. Assuming as the plane-strain problem in the present study, the unit thickness of the adherend is set as 1.

From the comparisons shown in Fig. A1, it can be found that the ultimate tensile loading F_u of the joint increases as the scarf angle θ decreases, in which the variation trends of the curves corresponding to the scarf angle θ have a good agreement with each other. Furthermore, it can also be observed that the ultimate tensile loading F_u of the joint increases as the adhesive thickness t_{ad} decreases. Thus, it can be concluded that the present simulated method is effective in analyzing the mechanical properties of the SJ under uniaxial tensile loading.

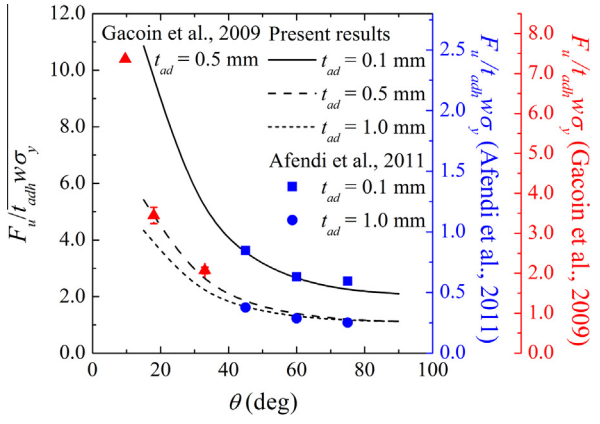

Fig. A1. Normalized loading plotted as a function of scarf angle: comparisons between the present results and the existing experimental measurements, taking different adhesive thicknesses into account.

References

Adams, R.D., Wake, W.C., Comyn, J., 1997. Structural Adhesive Joints in Engineering, second ed. Chapman & Hall, London.

Afendi, M., Teramoto, T., Bakri, H.B., 2011. Strength prediction of epoxy adhesively bonded scarf joints of dissimilar adherends. Int. J. Adhes. Adhes. 31, 402–411.

Campilho, R.D.S.G., de Moura, M.F.S.F., Ramantani, D.A., Morais, J.J.L., Domingues, J.J.M.S., 2009. Tensile behavior of three-dimensional carbon-epoxy adhesively bonded single- and double-strap repairs. Int. J. Adhes. Adhes. 29, 678–686.

Chai, H., 2004. The effects of bond thickness, rate and temperature on the deformation and fracture of structural adhesives under shear loading. Int. J. Fract. 130 (1), 497–515.

Chandra, N., Li, H., Shet, C., Ghonem, H., 2002. Some issues in the application of cohesive zone models for metal-ceramic interfaces. Int. J. Solids Struct. 39, 2827–2855.

de Moura, M.F.S.F., Goncalves, J.P.M., Chousal, J.A.G., Campilho, R.D.S.G., 2008. Cohesive and continuum mixed-mode damage models applied to the simulation of the mechanical behaviour of bonded joints. Int. J. Adhes. Adhes. 28, 419–426.

Freund, L.B., Suresh, S., 2003. Thin Film Materials: Stress, Defect Formation and Surface Evolution. Cambridge University Press, Cambridge.

Gacoin, A., Lestriez, P., Assih, J., Objois, A., Delmas, Y., 2009. Comparison between experimental and numerical study of the adhesively bonded scarf joint and double scarf joint: Influence of internal singularity created by geometry of the double scarf joint on the damage evolution. Int. J. Adhes. Adhes. 29, 572–579.

Ghosh, S., Ling, Y., Majumdar, B., Kim, R., 2000. Interfacial debonding analysis in multiple fiber reinforced composites. Mech. Mater. 32 (10), 561–591.

Gustafson, Peter A., Waas, Anthony M., 2009. The influence of adhesive constitutive parameters in cohesive zone finite element models of adhesively bonded joints. Int. J. Solids Struct. 46, 2201–2215.

Hamit, Adin, 2012. The investigation of the effect of angle on the failure load and strength of scarf lap joints. Int. J. Mech. Sci. 61, 24–31.

He, D., Sawa, T., Karami, A., 2009. Stress analysis and strength evaluation of scarf adhesive joints with dissimilar adherends subjected to static tensile loadings. JSME Int. J. Ser. A 3 (8), 1033–1044.

He, D., Sawa, T., Iwamoto, T., Hirayama, Y., 2010. Stress analysis and strength evaluation of scarf adhesive joints subjected to static tensile loadings. Int. J. Adhes. Adhes. 30, 387–392.

Ji, G.F., Ouyang, Z.Y., Li, G.Q., Ibekwe, S., Pang, S.S., 2010. Effects of adhesive thickness on global and local Mode-I interfacial fracture of bonded joints. Int. J. Solids Struct. 47 (18–19), 2445–2458.

Ji, G.F., Ouyang, Z.Y., Li, G.Q., 2011. Effects of bondline thickness on Mode-II interfacial laws of bonded laminated composite plate. Int. J. Fract. 168 (2), 197–207.

Ji, G.F., Ouyang, Z.Y., Li, G.Q., 2012. On the interfacial constitutive laws of mixed mode fracture with various adhesive thicknesses. Mech. Mater. 47, 24–32.

Kahraman, R., Sunar, M., Yilbas, B., 2008. Influence of adhesive thickness and filler content on the mechanical performance of aluminum single-lap joints bonded with aluminum powder filled epoxy adhesive. J. Mater. Process Tech. 205 (1–3), 183–189.

Kimiaeifar, A., Toft, H., Lund, E., Thomsen, O.T., Srensen, J.D., 2012. Reliability analysis of adhesive bonded scarf joints. Eng. Struct. 35, 281–287.

Lee, D.B., Ikeda, T., Miyazaki, N., Choi, N.S., 2004. Effect of bond thickness on fracture toughness of adhesive joints. J. Eng. Mater. Technol. 126, 14–18.

Lee, M.J., Cho, T.M., Kim, W.S., Lee, B.C., Lee, J.J., 2010. Determination of cohesive parameters for a mixed-mode cohesive zone model. Int. J. Adhes. Adhes. 30, 322–328.

Li, H., Chandra, N., 2003. Analysis of crack growth and crack-tip plasticity in ductile materials using cohesive zone models. Int. J. Plast. 19, 849–882.

Liechti, K.M., Freda, T., 1989. On the use of laminated beams for the determination of pure and mixed-mode fracture properties of structural adhesives. J. Adhes. 28, 145–169.

Banea, M.D., Lucas, F.M. da Silva, 2009. Mechanical characterization of flexible adhesives. J. Adhes. 85, 261–285.

Lucas, F.M. da Silva, Rodrigues, T.N.S.S., Figueiredo, M.A.V., de Moura, M.F.S.F., Chousal, J.A.G., 2006. Effect of adhesive type and thickness on the lap shear strength. J. Adhes. 82 (11), 1091–1115.

Lucas, F.M. da Silva, Gritchlow, G.W., Figueiredo, M.A.V., 2008. Parametric study of adhesively bonded joints. J. Adhes. Sci. Technol. 22, 1477–1494.

Lucas, F.M. da Silva, Carbas, R.J.C., Gritchlow, G.W., Figueiredo, M.A.V., Brown, K., 2009. Effect of material, geometry, surface treatment and environment on the shear strength of single lap joints. Int. J. Adhes. Adhes. 29, 621–632.

Marzi, S., Biel, A., Stigh, U., 2011. On experimental methods to investigate the effect of layer thickness on the fracture behavior of adhesively bonded joints. Int. J. Adhes. Adhes. 31, 840–850.

Mello, A.V., Liechti, K.M., 2006. The effect of self-assembled monolayers on interfacial fracture. J. Appl. Mech. 73, 860–870.

Mohammed, I., Liechti, K.M., 2000. Cohesive zone modeling of crack nucleation at bimaterial corners. J. Mech. Phys. Solids 48, 735–764.

Pardoen, T., Ferracin, T., Landis, C.M., Delannay, F., 2005. Constraint effects in adhesive joint fracture. J. Mech. Phys. Solids 53, 1951–1983.
Park, K., Paulino, G.H., 2011. Cohesive zone models: a critical review of traction–separation relationships across fracture surfaces. Appl. Mech. Rev. Trans. ASME 64, 061002.
Ridha, M., Tan, V.B.C., Tay, T.E., 2011. Traction–separation laws for progressive failure of bonded scarf repair of composite panel. Compos. Struct. 93, 1239–1245.
Rudawska, Anna, 2010. Adhesive joint strength of hybrid assemblies: titanium sheet-composites and aluminium sheet-composites – experimental and numerical verification. Int. J. Adhes. Adhes. 30, 574–582.
Sørensen, B.F., Kirkegaard, P., 2006. Determination of mixed mode cohesive laws. Eng. Fract. Mech. 73 (17), 2642–2661.
Sou-Hsiung, Jack Chiu, Reaz, A. Chaudhuri, 2011. A three-dimensional eigenfunction expansion approach for singular stress field near an adhesively-bonded scarf joint interface in a rigidly-encased plate. Eng. Fract. Mech. 78, 2220–2234.
Swadener, J.G., Liechti, K.M., 1998. Asymmetric shielding mechanisms in the mixed-mode fracture of a glass/epoxy interface. J. Appl. Mech. 65, 25–29.
Swadener, J.G., Liechti, K.M., de Lozanne, A.L., 1999. The intrinsic toughness and adhesion mechanism of a glass/epoxy interface. J. Mech. Phys. Solids 47, 223–258.
Wei, Y.G., Zhao, H.F., 2008. Peeling experiments of ductile thin films along ceramic substrates – critical assessment of analytical models. Int. J. Solids Struct. 45, 3779–3792.
Xu, W., Wei, Y., 2012. Strength and interface failure mechanism of adhesive joints. Int. J. Adhes. Adhes. 34, 80–92.
Xu, W., Wei, Y., 2013a. Influence of adhesive thickness on local interface fracture and overall strength of metallic adhesive bonding structures. Int. J. Adhes. Adhes. 40, 158–167.
Xu, W., Wei, Y., 2013b. Assessments for impact of adhesive properties: modeling strength of metallic single lap joint. J. Adhes. Sci. Technol. 27 (1), 9–29.
Yang, Q.D., Thouless, M.D., 2001. Mixed-mode fracture analyses of plastically-deforming adhesive joints. Int. J. Fract. 110, 175–187.